DFT-based comparative analysis of elastic, electronic, optical, and dynamic properties of PbS and PbSe crystals

Cite as: AIP Advances 15, 095120 (2025); doi: 10.1063/5.0293548
Submitted: 28 July 2025 • Accepted: 1 September 2025 •
Published Online: 16 September 2025

Nilufer Yesmin Tanisa,[1,a)] Nilanjana Sarker Nipa,[1,2] and Tanjila Akther Bhuiyan[1]

AFFILIATIONS

[1] Department of Physics, Uttara University, Uttara, Dhaka 1230, Bangladesh
[2] Dhaka Commerce College, Mirpur, Dhaka 1216, Bangladesh

[a)] **Author to whom correspondence should be addressed:** tanisha.90@uttarauniversity.edu.bd. **Tel.:** (+880) 1719509512

ABSTRACT

This study presents a comprehensive comparative analysis of the elastic, electronic, optical, and dynamic properties of lead chalcogenide semiconductors, lead sulfide (PbS) and lead selenide (PbSe), using density functional theory calculations. The structural stability and mechanical behavior were evaluated through elastic constants, revealing contrasting anisotropy and stiffness profiles. Electronic band structures and density of states highlighted significant differences in bandgap characteristics and carrier mobility potential. Optical investigations, including photoconductivity, absorption coefficient, reflectivity, and dielectric functions demonstrated PbSe's superior responsiveness in the ultraviolet range, while PbS exhibited more subdued optical activity, making it better suited for infrared applications. Dynamic properties such as phonon dispersion and density of states provided insights into lattice vibration modes and thermal transport tendencies. These multi-property comparisons underscore the functional versatility of PbS and PbSe and guide their suitability for optoelectronic, thermoelectric, and photonic applications.

I. INTRODUCTION

Lead chalcogenides, especially lead sulfide (PbS) and lead selenide (PbSe), have emerged as critical materials in thermoelectric, optoelectronics, and infrared (IR) technologies due to their semiconducting properties, narrow bandgaps, and favorable transport characteristics.[1–3] These compounds crystallize in a cubic rock salt (B1) structure and possess direct bandgaps at the L-point of the Brillouin zone, ~0.29 eV for PbS and 0.27 eV for PbSe at room temperature.[4] Their large dielectric constants and high exciton Bohr radii enable strong quantum confinement effects in nanostructured systems.[5]

Pioneering work by Cohen and Chelikowsky laid the groundwork in 1985, with investigations into band structures, densities of states, and x-ray photoemission spectra.[6] More recently, Wei and Zunger employed the Linearized Augmented Plane Wave (LAPW) method,[7,8] using both the Local Density Approximation (LDA)[9] and the Generalized Gradient Approximation (GGA-PBE),[10] to study lead chalcogenides in depth, capitalizing on modern high-performance computing systems to achieve accurate predictions.[11]

To improve performance and discover novel thermoelectric candidates, numerous studies have explored fundamental lattice dynamics. Experimental results revealed that PbS and PbSe exhibit strongly anharmonic behavior,[6–8] thermally induced atomic distortions,[6,8,12] and phonon scattering mechanisms, confirmed both experimentally and via molecular dynamics simulations.[13] Off-centering of Pb cations has also been observed even at moderate temperatures,[6,8] although the precise magnitude remains under debate.[12]

Band convergence, a key factor in improving thermoelectric efficiency, has been widely studied,[14–16] and thermal disorder's impact on electronic band structures has also been modeled.[13] First-principles Density Functional Theory (DFT) simulations[17] have contributed significantly to understanding the electronic structure,[18,19] lattice dynamics, and thermal conductivity.[20–24] In

addition, several studies have analyzed the effects of pressure[21,23] and temperature[13,22,25] on material properties.

Despite this wealth of work, many DFT studies rely on fixed lattice constants derived from experiment, which may not reflect the actual equilibrium geometry at varying temperatures. Since the lattice constant is sensitive to the choice of the functional, such approximations can misrepresent thermal states—especially in high-temperature thermoelectric systems such as PbTe. It is essential, therefore, to incorporate temperature effects explicitly to more accurately describe the material behavior.

This study presents a comprehensive comparative analysis of the elastic, electronic, optical, and dynamic properties of PbS and PbSe using DFT. By uncovering deeper structure–property relationships, we aim to guide the intelligent design of energy and sensing materials for next-generation technologies.

II. METHODOLOGY

Density Functional Theory (DFT) calculations were performed to investigate the elastic, electronic, optical, and dynamic properties of PbS and PbSe crystals. All simulations were carried out using the CASTEP module within the Materials Studio suite, employing a plane-wave pseudopotential approach. The Perdew–Burke–Ernzerhof (PBE) form of the Generalized Gradient Approximation (GGA)[10] was selected due to its proven balance between accuracy and computational efficiency for lead chalcogenides.[7,19] Norm-conserving pseudopotentials were used for Pb, S, and Se atoms. A plane-wave cutoff energy of 244.9 eV ensured reliable convergence of the total energy and stress tensors. A Monkhorst–Pack grid of 2 × 2 × 2 points was adopted for the primitive cubic cell of both PbS and PbSe to sample electronic states.[20] Both compounds were fully relaxed until the forces on each atom were below 0.01 eV/Å, with energy convergence set to 1×10^{-5} eV per atom. Optimization included both ionic positions and lattice parameters, calculated using finite-strain theory with applied deformations followed by stress analysis. The resulting stiffness tensor C_{ij} was used to derive bulk modulus, shear modulus, Poisson's ratio, and anisotropy indices. Band structure and density of states (DOS) were extracted along high-symmetry paths in the Brillouin zone. The calculated bandgaps and DOS profiles enabled assessment of carrier mobility and optoelectronic performance. Real and imaginary parts of the dielectric function, reflectivity, absorption coefficient, and energy-loss spectra were computed using the linear response formalism within CASTEP. Dynamic properties were derived using Density Functional Perturbation Theory (DFPT), enabling the analysis of lattice vibrations, phonon group velocity, and Debye temperature.[23,24]

III. RESULTS AND DISCUSSION

A. Electronic band structure and density of states (DOS)

Figure 1 shows the electrical band structures of PbS and PbSe and Fig. 2 presents the adjusted energy range for band structure comparison for PbS and PbSe, determined using Density Functional Theory (DFT). Both materials show semiconducting properties, with indirect bandgaps. PbS and PbSe are indirect bandgap semiconductors. PbS has an indirect bandgap of ~0.45 eV, with the

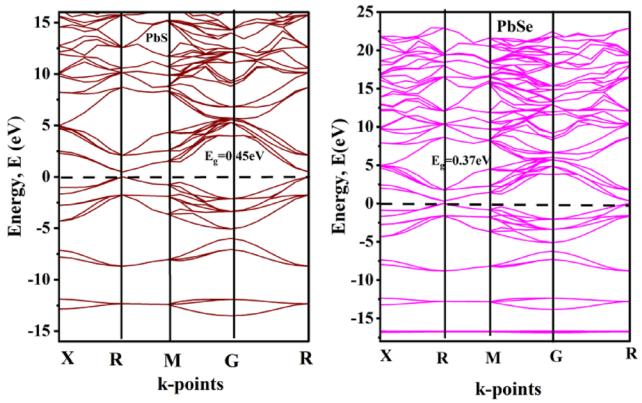

FIG. 1. The electrical band structures of PbS and PbSe.

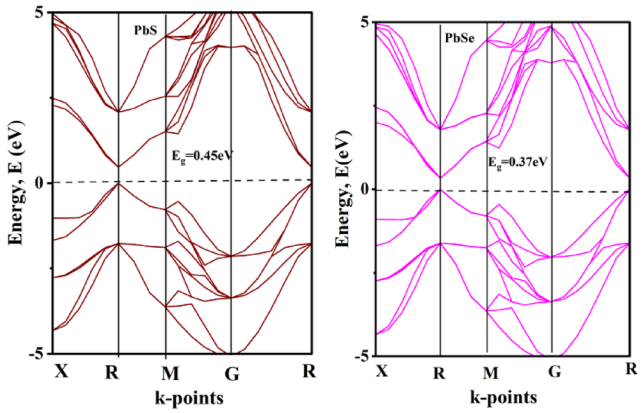

FIG. 2. Adjusted energy range for band structure comparison for PbS and PbSe.

conduction band minimum (CBM) located at the R-point and the valence band maximum (VBM) situated between the G and M points. Similarly, PbSe also exhibits an indirect bandgap, with the CBM and VBM located at distinct k-points along the Brillouin zone, resulting in a slightly lower bandgap of around 0.37 eV. These figures confirm the narrow-bandgap semiconductor properties of these lead chalcogenides and are in line with earlier theoretical reports.[26,27] The p-orbitals of the chalcogen atoms (S and Se) in both compounds are the main source of the valence bands, while the lead (Pb) p-orbitals dominate the conduction bands. PbSe exhibits a somewhat higher carrier mobility than PbSe due to a more prominent dispersion near the Fermi level. These electrical characteristics demonstrate how PbS and PbSe's adjustable band topologies and appropriate bandgaps make them promising for optoelectronic and thermoelectric applications.

The total density of state (DOS) and partial density of states (PDOS) of PbS and PbSe are illustrated in Fig. 3, providing detailed insights into the contributions of various atomic orbitals to the electronic structure near the Fermi level. The DOS plot for PbS shows a significant total DOS peak around −20 eV, primarily due to the Pb-5d orbitals, as indicated in the lower PDOS panel. These deep-lying

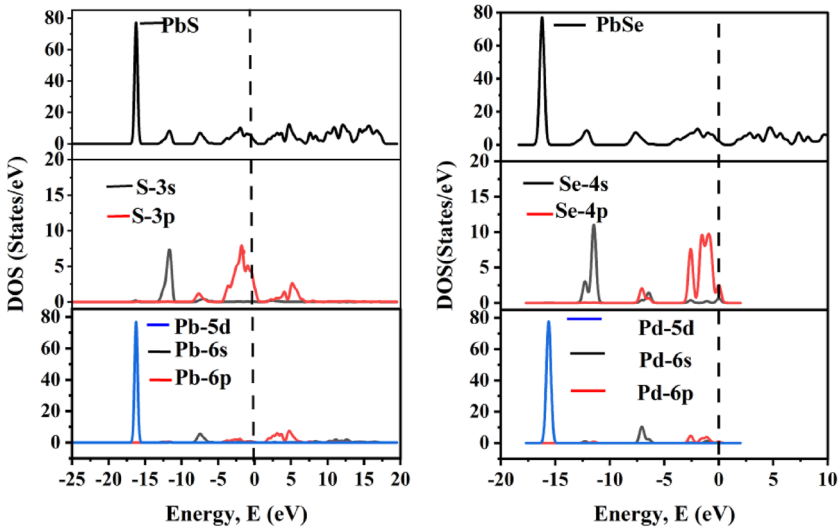

FIG. 3. Density of states (DOS) of PbS and PbSe.

states are well separated from the valence and conduction bands and do not participate directly in the electronic transitions near the Fermi level. The S-3p orbitals (middle panel) dominate the valence band region between −8 and 0 eV, while the Pb-6p states make a major contribution near the conduction band minimum (CBM). The S-3s states appear around −15 eV, indicating their deep-core nature, and the Pb-6s orbitals contribute slightly below the Fermi level. The Fermi energy is aligned at 0 eV, with no states crossing it, confirming the semiconducting nature of PbS. The strong overlap between S-3p and Pb-6p orbitals near the Fermi level reflects a strong p–p hybridization, which governs the electronic transport behavior of PbS. For PbSe, a similar electronic configuration is observed. A sharp peak in the total DOS around −15 eV corresponds to the localized Pb-5d orbitals. The Se-4p orbitals, similar to the sulfur counterpart in PbS, dominate the valence region just below the Fermi level, especially from −5 to 0 eV. The conduction band edge is primarily formed by the Pb-6p states, with minor contributions from Pb-6s. The DOS analysis confirms that the valence band edges are mainly derived from the anion p-orbitals (S-3p and Se-4p), while the conduction band edges originate from the Pb-6p orbitals. The strong p–p hybridization and semiconducting nature of both PbS and PbSe make them promising candidates for optoelectronic and thermoelectric applications.

B. Dynamic properties

For PbS (lead sulfide), the dispersion graph (Fig. 4) shows acoustic branches that begin at zero frequency at the G point, gradually increasing along the symmetry paths (X–R–M–G–R). The optical phonon modes reach up to ~7 THz, suggesting strong interatomic forces and relatively stiff Pb–S bonds. The separation between acoustic and optical branches is distinct, which typically

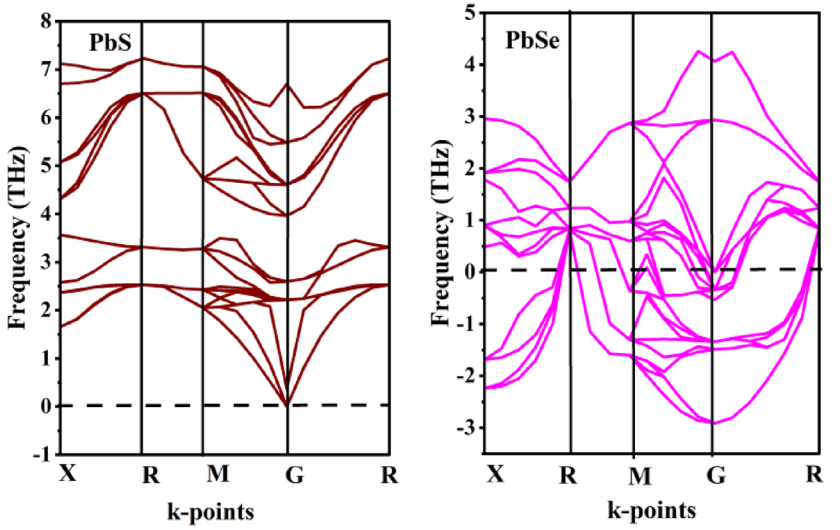

FIG. 4. Phonon dispersion curves of PbS and PbSe.

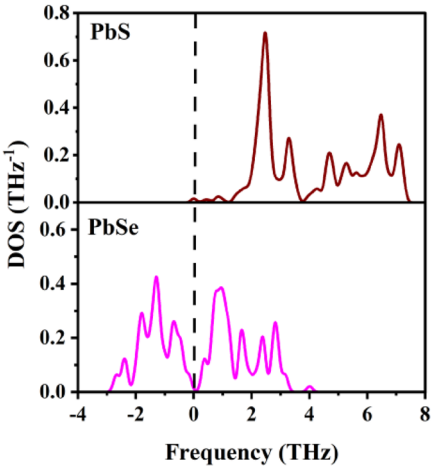

FIG. 5. Vibrational density of states (VDOS) of PbS and PbSe.

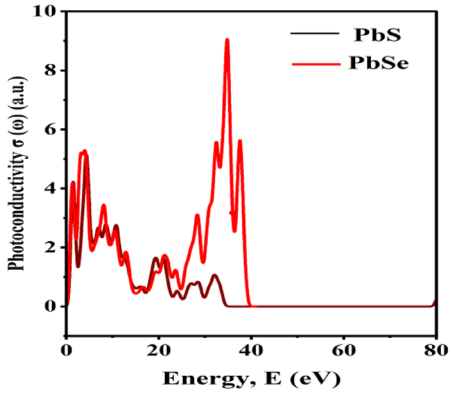

FIG. 6. Photoconductivity spectra of PbS and PbSe.

points to minimized phonon scattering and potential for good thermal conductivity. As shown in Fig. 4, PbSe (lead selenide) exhibits a more subdued phonon activity. The acoustic modes rise slowly in frequency, and optical branches reach only about 4.5 THz. Notably, certain regions of the dispersion curve for PbSe reveal imaginary frequencies (represented as negative values).

In Fig. 5, PbS presents a prominent peak in DOS around 6 THz, indicating a high density of optical phonon modes contributing at that frequency. This confirms the relatively high frequency nature of its phonon modes and potential for vibrational energy dispersion. PbSe, however, has a lower and broader peak at ~2 THz, signifying a heavier contribution from low-frequency vibrations. PbS demonstrates stronger lattice vibrations and stiffer bonding characteristics, with phonon modes concentrated at higher frequencies. PbSe shows signs of instability and softer lattice dynamics, reflected in its broader and lower DOS profile. These vibrational properties influence key material characteristics such as thermal conductivity, specific heat capacity, and electron–phonon interactions, making phonon analysis essential for tailoring these materials in optoelectronic or thermoelectric applications.

We observed the presence of imaginary frequencies in the phonon spectrum of PbSe, particularly in certain regions of the dispersion curve. These imaginary frequencies are indicative of potential lattice instabilities, suggesting that PbSe may experience softening of its lattice under certain conditions. Such instabilities could affect the material's mechanical stability, which is crucial for its performance in practical applications. The implications of these phonon modes on PbSe's structural integrity and its long-term reliability in optoelectronic devices warrant further investigation. Future work should focus on understanding the temperature and pressure dependence of these imaginary frequencies and exploring potential strategies to mitigate their impact on the material's stability.

C. Photoconductivity

As shown in Fig. 6, PbSe exhibits significantly stronger photoconductive responses than PbS, especially in the 30–50 eV range, where its conductivity peaks surpass nine arbitrary units. This indicates that PbSe has a highly efficient mechanism for exciting charge carriers and a favorable band structure for absorbing high-energy photons. Its strong sensitivity in the extreme ultraviolet (EUV) region makes it well suited for advanced applications such as high-energy photodetectors and x-ray sensing devices. In contrast, PbS shows a weaker and more diffuse photoconductive response, suggesting lower charge carrier mobility or shorter carrier lifetimes after excitation. This reduced activity implies that PbS is more appropriate for low-energy applications such as infrared detection. The stark difference in their photoconductive behavior highlights the critical role of material selection based on the desired spectral range and confirms PbSe's superiority for high-energy optoelectronic technologies.

D. Refractive index

Figure 7 presents the energy-dependent refractive index and extinction coefficient of PbS and PbSe. The real part of the refractive index n(ω) and the extinction coefficient k(ω) of PbS and PbSe exhibit contrasting optical behaviors. Initially, PbSe displays a higher refractive index (~7 at 0 eV) than PbS (~6.5), although both materials gradually decrease and stabilize around 2.5 beyond 40 eV, suggesting diminished optical dispersion and reduced bound electronic contributions. The extinction coefficient, which indicates the degree of light absorption, begins at a high value for both materials—~3.5 for PbSe and ~2.5 for PbS—but also trends downward with increasing photon energy, stabilizing near 0.5 past 40 eV. These trends highlight that while PbSe has stronger initial optical confinement and absorption characteristics, both compounds converge in behavior at high energies, making them suitable for tailored optoelectronic applications across infrared and ultraviolet regimes.

E. Reflectivity and loss function

As shown in Fig. 8, PbSe exhibits notably stronger reflectivity, reaching a peak value close to 0.8 around 40 eV, whereas PbS remains below 0.4 throughout the range, with only subtle features. This difference suggests that PbSe has a much higher surface reflectivity and potentially stronger light–electron interaction than PbS, especially in the high-energy region. Complementary to this, the energy loss function L(ω), which represents the energy loss of fast

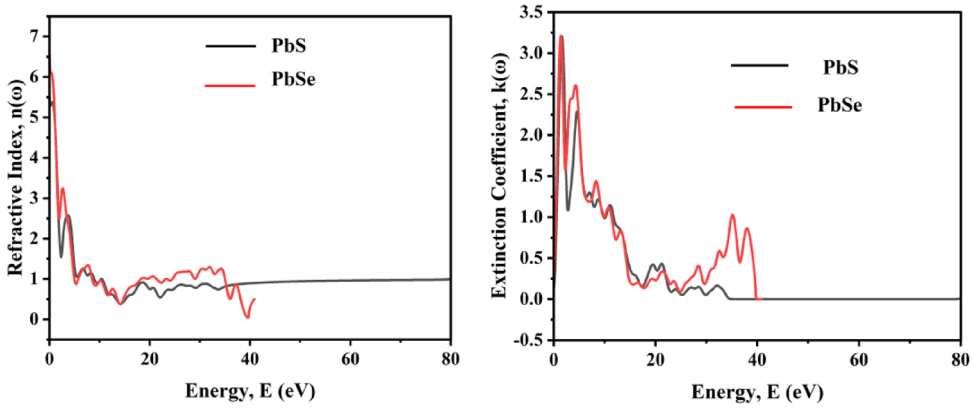

FIG. 7. Energy-dependent refractive index and extinction coefficient of PbS and PbSe.

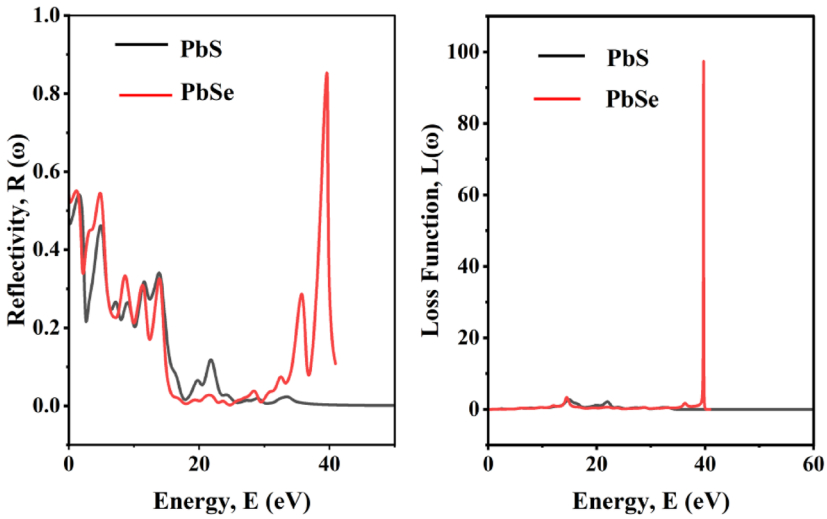

FIG. 8. Energy-resolved reflectivity and electron energy-loss spectra of PbS and PbSe.

electrons traversing the material, shows a sharp and dominant peak near 40 eV for PbSe, approaching values close to 100. In contrast, PbS's loss peak is significantly weaker and remains below 20, indicating lower plasmonic activity. Together, these observations imply that PbSe has stronger collective electronic oscillations (plasmons) and is more optically active, making it a more promising candidate for plasmonic and photonic applications in the extreme ultraviolet regime. PbS, while still viable, may be less effective in high-energy light management technologies where strong reflectivity and loss characteristics are required.

F. Dielectric function

Figure 9 shows the real and imaginary components of the dielectric function for PbS and PbSe. For the real dielectric constant $\varepsilon_r(\omega)$, both materials begin with high values, ~40 for PbS and slightly higher for PbSe, indicating strong polarization under an electric field at low energies. As energy increases, $\varepsilon_r(\omega)$ rapidly decreases, stabilizing near zero beyond 20 eV, which marks the diminishing ability of these materials to sustain bound electronic states. This decline is indicative of the material's transition from a dispersive medium to a more absorptive regime. The imaginary part of the dielectric constant $\varepsilon_i(\omega)$, associated with absorption, similarly shows high initial values (about 25 for PbS, marginally higher for PbSe), but falls sharply with increasing energy. This trend suggests that both PbS and PbSe experience significant optical absorption at lower photon energies, making them effective in photovoltaic and infrared sensing applications. PbSe's slightly greater values in both real and imaginary components reflect its stronger dielectric response overall, suggesting better suitability for high-performance optoelectronic devices. Together, the dielectric profiles of PbS and PbSe point to their potential for energy harvesting and photonic applications. PbSe's stronger dielectric behavior could make it the preferred candidate in designs requiring a high refractive index and absorption efficiency.

G. Absorption coefficient

Figure 10 presents the optical absorption coefficient spectra of PbS and PbSe. PbSe demonstrates markedly higher absorption, with pronounced peaks particularly evident around 40 eV, reaching up to ~6×10^5 arbitrary units. In contrast, PbS exhibits more moderate absorption, with values ranging from about 1×10^5 to 2×10^5, and a smoother spectral profile. These variations suggest that PbSe has a stronger capability for photon absorption, likely due

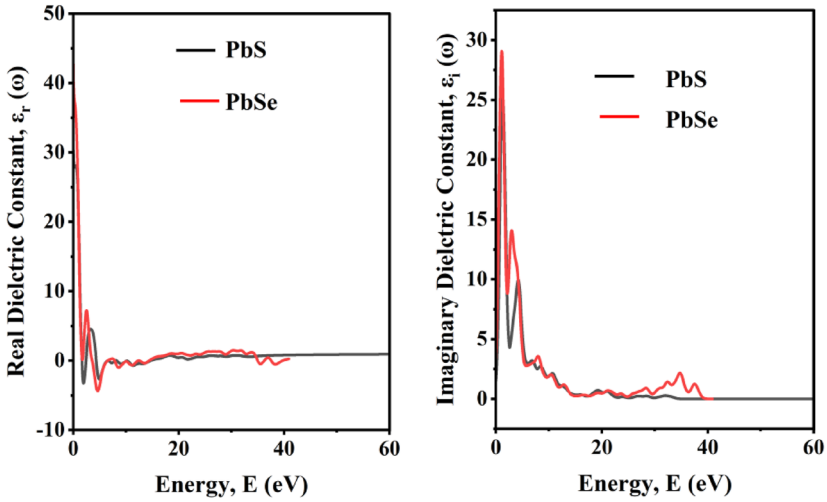

FIG. 9. Real and imaginary components of the dielectric function for PbS and PbSe.

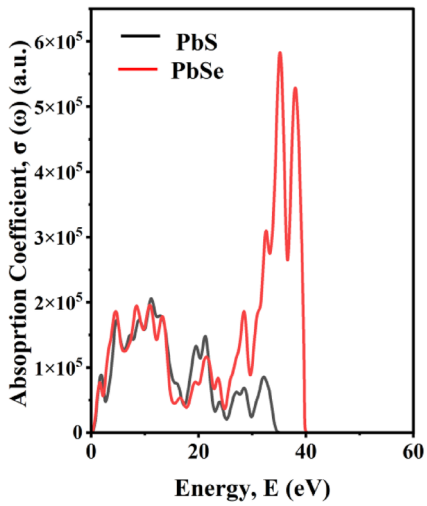

FIG. 10. Optical absorption coefficient spectra of PbS and PbSe.

to its favorable band structure and higher transition probabilities. Such enhanced absorption implies PbSe's suitability for applications requiring efficient light detection and conversion such as ultraviolet photodetectors and high-energy optical devices. On the other hand, the gentler absorption characteristics of PbS may be advantageous in infrared detection or in systems where reduced photon interaction is desired. This comparative analysis underscores the distinct optoelectronic potentials of each material.

H. Elastic properties

The strength and compressibility of material are defined by its elastic properties when submitted to a given amount of external pressure. In this study, due to their cubic system, the materials have only three independent elastic parameters (C_{11}, C_{12}, and C_{44}) for PbS and PbSe. We have applied the method, and the combinations of

TABLE I. The calculated values of the elastic constants (C_{ij} in GPa) at equilibrium for the PbS and PbSe compounds.

	C_{11}	C_{12}	C_{44}
	PbS		
Present	122	24	16
Expt.[a]	124	33	23
	PbSe		
Present	148	13	11
Expt.[b]	123.7	19.3	15.9

[a]Reference 28.
[b]Reference 29.

C_{ij} are calculated and presented in Table I. Therefore, the results of this study, which is predictive, have been compared to other theoretical calculations. Our results have been compared with the values found in the literature. Three separate elastic constants, C_{11}, C_{12}, and C_{44}, can be calculated by applying appropriate lattice distortions to a cubic lattice. To calculate the elastic constants, the following three equations are used:

$$B_0 = (C_{11} + 2C_{12})/3,$$

$$\Delta E_{rhomb} = \frac{1}{6}(C_{11} + 2C_{12} + 4C_{44})V_0\delta^2,$$

$$\Delta E_{tetra} = (C_{11} - C_{12})\ V_0\delta^2.$$

The bulk modulus B_0 is calculated using Murnaghan's equation of state. The first equation expresses the relationship between the elastic constants (C_{11} and C_{12}) and B_0. The second equation compares the strain energy (ΔE_{rhomb}) with the volume-conserving rhombohedral strain (δ). The third equation relates the fluctuation of the strain energy (ΔE_{tetra}) vs the volume conserving tetragonal strain (δ). The estimated elastic constants for the PbS and PbSe

compounds are shown in Table 1 and compared to experimental results. The computed values are consistent with the existing experimental data. The structural stability in a cubic crystal requires elastic constants satisfying the conditions $C_{11} - C_{12} > 0$, $C_{44} > 0$, $C_{11} + 2C_{12} > 0$, and $C_{12} < B_0 < C_{11}$. According to Table I, all these conditions are satisfied.

IV. CONCLUSION

This study conducted a comprehensive Density Functional Theory (DFT) analysis of PbS and PbSe, revealing key contrasts and complementarities across their elastic, electronic, optical, and dynamic behaviors. The optimized elastic constants demonstrated greater stiffness in PbSe, with C_{11} = 148 GPa compared to 122 GPa for PbS, indicating PbSe's higher mechanical resilience. The electronic bandgap values—0.45 eV for PbS and 0.37 eV for PbSe—confirmed their narrow-gap semiconducting nature, suggesting strong infrared and thermoelectric applicability. Optical properties further emphasized material differentiation: PbSe exhibited a superior refractive index (~7 at 0 eV), peak reflectivity nearing 0.8, and an absorption coefficient that reached up to 6×10^5 units around 40 eV, almost triple that of PbS. The dielectric function results reaffirm PbSe's stronger polarization and absorption capabilities, solidifying its role in UV and EUV photonics. Dynamic properties showed PbS's stiffer phonon modes (~7 THz), in contrast to PbSe's broader and lower frequency range, reflecting softer lattice dynamics and imaginary frequencies indicative of potential instabilities. Together, these findings establish PbSe as being better suited for high-energy optoelectronic and plasmonic applications, while PbS's stable vibrational properties and moderate optical activity make it ideal for infrared sensing and thermoelectric systems. These insights provide valuable guidance for tailoring lead chalcogenide-based materials in advanced photonic and energy conversion technologies.

ACKNOWLEDGMENTS

The authors extend their heartfelt appreciation to the Department of Physics, Uttara University, situated at Holding 77, Beribadh Road, Turag, Uttara, Dhaka-1230, Bangladesh, for their steadfast support throughout this research. The invaluable resources and assistance provided by the department greatly contributed to the thoroughness and excellence of this study.

AUTHOR DECLARATIONS

Conflict of Interest

The authors have no conflicts to disclose.

Author Contributions

Nilufer Yesmin Tanisa conceptualized and designed the study, created and illustrated the graphical representations, systematically gathered and interpreted the data, and drafted the manuscript. Nilanjana Sarker Nipa and Tanjila Akther Bhuiyan played pivotal roles in conducting the theoretical analysis, performing a detailed evaluation of the data, and collaboratively contributing to the drafting and refinement of the manuscript.

Nilufer Yesmin Tanisa: Conceptualization (equal); Investigation (equal); Methodology (equal); Software (equal); Writing – original draft (equal). **Nilanjana Sarker Nipa**: Software (equal); Writing – review & editing (equal). **Tanjila Akther Bhuiyan**: Visualization (equal); Writing – review & editing (equal).

DATA AVAILABILITY

Data sharing is not applicable to this article as no new data were created or analyzed in this study.

REFERENCES

[1] I. I. Ravich, *Semiconducting Lead Chalcogenides* (Springer Science & Business Media, 2013), Vol. 5.
[2] M. R. Shankar and A. N. Prabhu, "A review on structural characteristics and thermoelectric properties of mid-temperature range Chalcogenide-based thermoelectric materials," J. Mater. Sci. **58**(43), 16591–16633 (2023).
[3] V. Patterson, "Band gap study of lead chalcogenide alloys," Doctoral dissertation (University of Wollongong, 2017).
[4] H. A. Morris, *Investigation of the Optical Properties of PbSe/PbX Nanocrystals for Photodetector Applications* (University of Arkansas, 2016).
[5] Y. Benchérif, A. Boukra, A. Zaoui, and M. Ferhat, "High-pressure phases of lead chalcogenides," Mater. Chem. Phys. **126**(3), 707–710 (2011).
[6] M. L. Cohen and J. R. Chelikowsky, *Electronic Structure and Optical Properties of Semiconductors* (Springer Science & Business Media, 2012), Vol. 75.
[7] S. H. Wei and A. Zunger, "Electronic and structural anomalies in lead chalcogenides," Phys. Rev. B **55**(20), 13605 (1997).
[8] O. K. Andersen, "Linear methods in band theory," Phys. Rev. B **12**(8), 3060 (1975).
[9] D. J. Singh and L. Nordström, *Planewaves, Pseudopotentials and the LAPW Method* (Springer US, Boston, MA, 2006).
[10] J. P. Perdew and A. Zunger, "Self-interaction correction to density-functional approximations for many-electron systems," Phys. Rev. B **23**(10), 5048 (1981).
[11] J. P. Perdew, K. Burke, and M. Ernzerhof, "Generalized gradient approximation made simple," Phys. Rev. Lett. **77**(18), 3865 (1996).
[12] Z. Sohrabikia, M. Jafari, and B. A. Ravan, "Strain engineering of electrical and optical properties of two dimensional hexagonal PbX (X = S, Se) monolayers," Comput. Theor. Chem. **1244**, 115004 (2025).
[13] Y. Zhang, X. Ke, C. Chen, J. Yang, and P. R. C. Kent, "Thermodynamic properties of PbTe, PbSe, and PbS: First-principles study," Phys. Rev. B **80**(2), 024304 (2009).
[14] O. Kilian, G. Allan, and L. Wirtz, "Near Kohn anomalies in the phonon dispersion relations of lead chalcogenides," Phys. Rev. B **80**(24), 245208 (2009).
[15] J. Hoja, A. M. Reilly, and A. Tkatchenko, "First-principles modeling of molecular crystals: Structures and stabilities, temperature and pressure," Wiley Interdiscip. Rev.: Comput. Mol. Sci. **7**(1), e1294 (2017).
[16] Y. W. Tsang and M. L. Cohen, "Calculation of the temperature dependence of the energy gaps in PbTe and SnTe," Phys. Rev. B **3**(4), 1254 (1971).
[17] J. M. Skelton, S. C. Parker, A. Togo, I. Tanaka, and A. Walsh, "Thermal physics of the lead chalcogenides PbS, PbSe, and PbTe from first principles," Phys. Rev. B **89**(20), 205203 (2014).
[18] P. Hohenberg and W. Kohn, "Inhomogeneous electron gas," Phys. Rev. **136**(3B), B864 (1964).
[19] W. F. Li, C. M. Fang, M. Dijkstra, and M. A. Van Huis, "The role of point defects in PbS, PbSe and PbTe: A first principles study," J. Phys.: Condens. Matter **27**(35), 355801 (2015).
[20] J. M. An, A. Franceschetti, S. V. Dudiy, and A. Zunger, "The peculiar electronic structure of PbSe quantum dots," Nano Lett. **6**(12), 2728–2735 (2006).
[21] T. Chattopadhyay, A. Werner, H. G. von Schnering, and J. Pannetier, "Temperature and pressure induced phase transition in IV-VI compounds," Rev. Phys. Appl. **19**(9), 807–813 (1984).
[22] Y. L. Pei and Y. Liu, "Electrical and thermal transport properties of Pb-based chalcogenides: PbTe, PbSe, and PbS," J. Alloys Compd. **514**, 40–44 (2012).

[23]Y. Zhang and W. J. Weber, "Role of energy partitioning on electron-hole recombination, trapping, and detection in silicon detectors," Phys. Rev. B **82**(7), 075202 (2010).
[24]G. Zhang and Y. W. Zhang, "Thermoelectric properties of two-dimensional transition metal dichalcogenides," J. Mater. Chem. C **5**(31), 7684–7698 (2017).
[25]S. K. Muzakir, "A study on the optoelectronic properties of lead chalcogenides nanospheres using a combination of experimental and theoretical approach," Malays. J. Microsc. **16**(1), 1 (2020).
[26]S. Aminorroaya Yamini, V. Patterson, and R. Santos, "Band-gap nonlinearity in lead chalcogenide (PbQ, Q = Te, Se, S) alloys," ACS Omega **2**(7), 3417–3423 (2017).
[27]S. A. Khan, Z. H. Khan, A. A. El-Sebaii, F. M. Al-Marzouki, and A. A. Al-Ghamdi, "Structural, optical and electrical properties of cadmium-doped lead chalcogenide (PbSe) thin films," Physica B **405**(16), 3384–3390 (2010).
[28]J. Han, S. Luo, X. Yin, Y. Zhou, H. Nan, J. Li, X. Li, D. Oron, H. Shen, and H. Lin, "Hybrid PbS quantum-dot-in-perovskite for high-efficiency perovskite solar cell," Small **14**(31), 1801016 (2018).
[29]P. B. Green, F. Y. Villanueva, K. Z. Demmans, C. J. Imperiale, M. Hasham, E. Nikbin, J. Y. Howe, D. C. Burns, and M. W. Wilson, "PbS nanocrystals made using excess lead chloride have a halide-perovskite-like surface," Chem. Mater. **33**(23), 9270–9284 (2021).